Galectin-1 is essential in tumor angiogenesis and is a target for antiangiogenesis therapy

Victor L. J. L. Thijssen*, Ruben Postel†, Ricardo J. M. G. E. Brandwijk*, Ruud P. M. Dings‡, Irina Nesmelova‡, Sietske Satijn*, Nicole Verhofstad*, Yusaku Nakabeppu§, Linda G. Baum¶, Jeroen Bakkers†, Kevin H. Mayo‡, Françoise Poirier‖, and Arjan W. Griffioen*,**

*Angiogenesis Laboratory, Research Institute for Growth and Development (GROW), Department of Pathology, University Maastricht, 6202 A2, Maastricht, The Netherlands; †Netherlands Institute for Developmental Biology and Interuniversity Cardiology Institute of the Netherlands, Hubrecht Laboratory, 3584 CT, Utrecht, The Netherlands; ‡Department of Biochemistry, Molecular Biology and Biophysics, University of Minnesota, Minneapolis, MN 55455; §Division of Neurofunctional Genomics, Department of Immunobiology and Neuroscience, Medical Institute of Bioregulation, Kyushu University, Fukuoka 812-8582, Japan; ¶Department of Pathology and Laboratory Medicine, School of Medicine, University of California, Los Angeles, CA 90095; and ‖Institut Jacques Monod, Unité Mixte de Recherche, Centre National de la Recherche Scientifique, 7592, Universités P6 and P7, 75251 Paris, France

We describe that galectin-1 (gal-1) is a receptor for the angiogenesis inhibitor anginex, and that the protein is crucial for tumor angiogenesis. gal-1 is overexpressed in endothelial cells of different human tumors. Expression knockdown in cultured endothelial cells inhibits cell proliferation and migration. The importance of gal-1 in angiogenesis is illustrated in the zebrafish model, where expression knockdown results in impaired vascular guidance and growth of dysfunctional vessels. The role of gal-1 in tumor angiogenesis is demonstrated in gal-1-null mice, in which tumor growth is markedly impaired because of insufficient tumor angiogenesis. Furthermore, tumor growth in gal-1-null mice no longer responds to antiangiogenesis treatment by anginex. Thus, gal-1 regulates tumor angiogenesis and is a target for angiostatic cancer therapy.

angiostatic therapy | endothelial cell | galectin | tumor models | anginex

An adequate vasculature is a prerequisite for tumors to grow, and the need for neovessel formation (or angiogenesis) provides a target for treatment of cancer (1). Endothelial cells (EC) that line the tumor vasculature are particularly suitable target cells for therapeutic approaches, because they are easily accessible to agents delivered by the blood (2). However, to affect only tumor vasculature, specific targets on angiogenically active EC are essential. To date, only a few targets of tumor vasculature have been identified (3).

We recently developed the specific angiostatic peptide anginex, which inhibits tumor growth through specific inhibition of angiogenesis (4–6). Although a broad profile of activities of anginex is known, such as prevention of EC adhesion and induction of apoptosis, the molecular target on tumor EC was never identified. In a receptor-finding study using a yeast two-hybrid screening approach, we identified galectin-1 (gal-1) as a target protein of anginex.

gal-1 belongs to a family of carbohydrate-binding proteins that share a conserved carbohydrate recognition domain of ≈130 aa (7–9). Over a dozen mammalian galectins have been described (10, 11), and members of this family are expressed in a wide range of species, suggesting an important role for galectins in basic cellular mechanisms. Galectins can be secreted and, depending on the cell type or state of differentiation, they have been found in the nucleus, cytoplasm, or extracellular matrix. It has been proposed that gal-1 mediates cell adhesion and migration (12) and is involved in several processes, including proliferation (13), apoptosis (14), and even mRNA splicing (15). The role of gal-1 in EC function or vascular biology has not been extensively studied.

Here, we describe the function of gal-1 in angiogenesis. We provide direct functional evidence that gal-1 is required for tumor angiogenesis and outgrowth of tumors. Furthermore, we show that gal-1 is the target for the potent angiogenesis inhibitor anginex, thus establishing gal-1 as an important target for anticancer therapy.

Results

gal-1 Binds the Angiostatic Peptide Anginex. The goal of the present study was to identify the receptor of anginex, an angiogenesis inhibitor previously shown to specifically target tumor EC (5). Immunohistochemistry revealed vesicular uptake of anginex by EC within 2 h (Fig. 1A). Electron microscopy showed anginex located at the membrane of intracellular vesicles, suggesting receptor-mediated uptake (Fig. 1B). To identify this receptor, yeast two-hybrid (Y2H) analysis was performed. To that end, the recently described artificial anginex gene (16) was cloned in-frame with the GAL-4 DNA-binding domain of the Y2H bait vector pGBDT7, which was confirmed by Western blotting (data not shown). Multiple screens against cDNA libraries of activated EC identified gal-1 as the receptor for anginex (see also *Supporting Text*, Table 1, and Fig. 5, which are published as supporting information on the PNAS web site), which was independently confirmed by using three approaches. (*i*) Double staining of anginex-treated EC showed colocalization of anginex and gal-1. (*ii*) Analysis of NMR spectra revealed chemical-shift changes of certain resonances from gal-1 upon addition of anginex, indicative of a specific molecular interaction. (*iii*) Plasmon resonance spectroscopy (BIAcore analysis) was used to further define the kinetics and stoichiometry of the interaction. Analysis of the binding kinetics revealed a 1:1 Langmuir association with a rate constant (k_a) of $\approx 6.5 \times 10^3$ Ms^{-1}, whereas the dissociation kinetics followed a biphasic pattern with dissociation rate constants of $4.2 \times 10^{-2} \cdot s^{-1}$ and $5.9 \times 10^{-4} \cdot s^{-1}$, respectively. These data suggest that dimerized anginex binds to gal-1, and that subsequently the two anginex molecules dissociate as monomers with a K_d of 6.4 μM for dissociation of first anginex molecule and a K_d of 90 nM for the second molecule. This result is supported by mass spectrometry, which displayed a major peak with a mass of 22.8 kDa [gal-1 monomer (14.7 kDa) + anginex dimer (8 kDa); data not shown]. The data above show that gal-1 and anginex interact, suggestive of gal-1 serving as receptor for anginex.
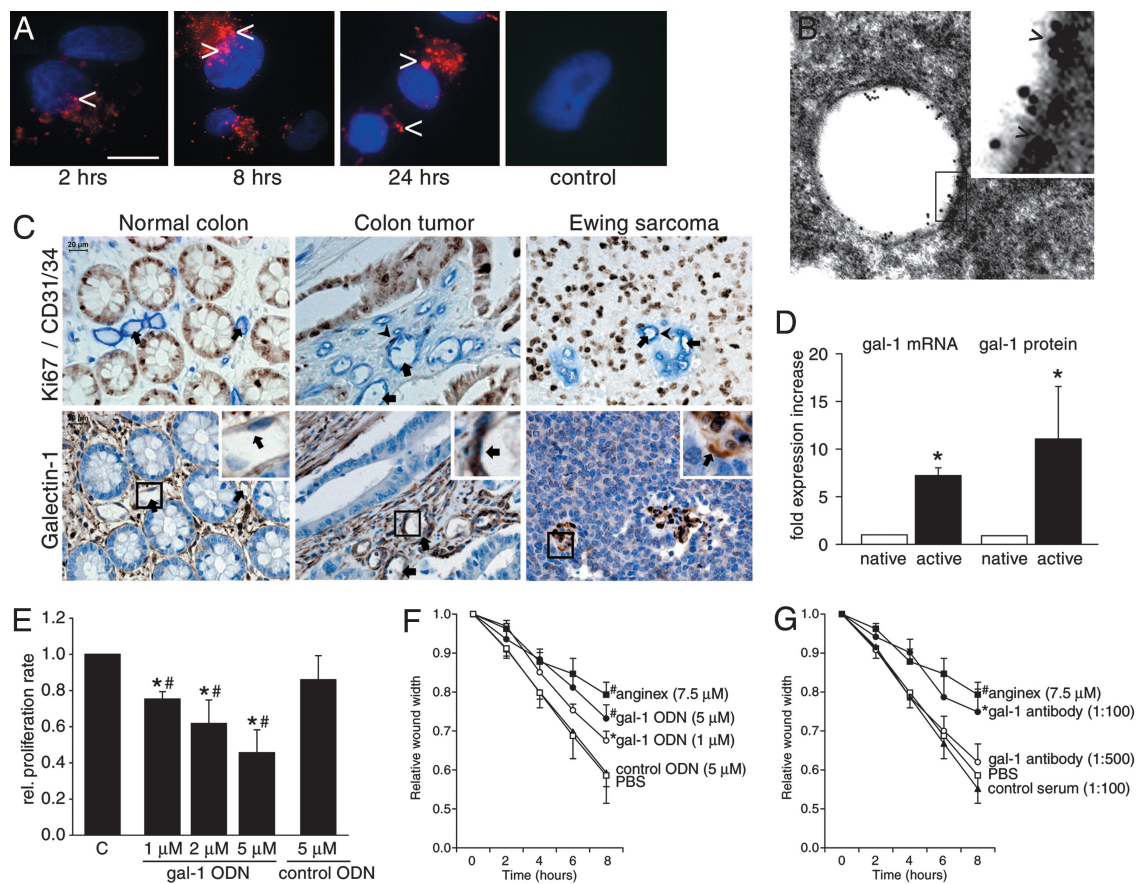
MEDICAL SCIENCES

Fig. 1. gal-1 binds to anginex, and gal-1 expression is enhanced in activated EC and tumor EC; role in EC function. (*A*) Immunohistochemical detection of anginex-treated HUVEC by using mouse monoclonal 2D10 anti-anginex antibody (red staining) in a time-lapse experiment. Nuclei are counterstained with DAPI (blue staining). Anginex appears in vesicular structures (arrowheads). In the control, the primary antibody was omitted. (Scale bar, 10 μm.) (*B*) Electron microscopy of an immunogold labeling of anginex demonstrating the accumulation of anginex in HUVEC. (*Inset*) Detail showing the membrane localization of anginex (arrowheads; ×80,500). (*C*) gal-1 is overexpressed in EC of human colon carcinoma as compared with normal human colon and in Ewing sarcoma. (*Upper*) Double staining for the EC (CD31/34, blue) and the proliferation marker Ki67 (brown/black). (*Lower*) Staining of a consecutive section for gal-1 (brown) with hematoxylin as counterstain (blue). The arrows indicate blood vessels. Arrowheads point toward individual proliferating EC. (*Insets*) Detail of gal-1 staining in EC (arrow). (*D*) gal-1 mRNA (qPCR; $n = 5$) and protein (FACS; $n = 4$) expression are up-regulated in activated HUVEC. Expression was determined in cells immediately after isolation from the umbilical vein (native) and after culturing the cells for 3 additional days in medium containing 20% human serum (active). *, $P < 0.05$. vs. native. (*E*) Knockdown of gal-1 expression with ODN results in a concentration-dependent inhibition of EC proliferation ($n = 4$); *, $P < 0.05$ vs. control; #, $P < 0.05$ vs. control ODN. (*F*) Treatment with 1 or 5 μM gal-1 ODN results in a significant inhibition of EC migration ($n = 4$); #, $P < 0.005$ vs. PBS; *, $P < 0.05$ vs. PBS. (*G*) Treatment with a gal-1 antibody results in a significant inhibition of EC migration ($n = 3$); #, $P < 0.005$ vs. PBS; *, $P < 0.01$ vs. PBS.

gal-1 Is Overexpressed in Tumor EC; a Crucial Role in EC Proliferation and Migration. To determine the role of gal-1 in tumor EC biology, we first analyzed gal-1 expression in human tumor blood vessels by immunohistochemistry. Although gal-1 is only weakly expressed in EC of normal tissue (the colon is shown: Fig. 1*C Left*), a strong expression was found in EC of human colon carcinoma (Fig. 1*C Center*) and breast carcinoma (data not shown), especially in EC that stained positive for the proliferation marker Ki67. Similar results were observed for a sarcoma type of tumor (Ewing sarcoma) in which the gal-1 staining was almost exclusively observed in vessels (Fig. 1*C Right*). These data demonstrate that the amount of gal-1 protein is up-regulated in angiogenically active EC. Indeed, growth factor activation of freshly isolated human umbilical vein EC (HUVEC) resulted in a significant increase in gal-1 mRNA expression and a concomitant >10-fold induction of gal-1 protein expression (Fig. 1*D*). Furthermore, treatment of activated EC with a gal-1 specific antisense oligodeoxynucleotide (ODN) resulted in inhibition of EC proliferation, whereas a random ODN had no effect (Fig. 1*E*). Besides EC proliferation, EC migration was also inhibited by treatment with either the gal-1-specific ODN (Fig. 1*F*) or the

rabbit polyclonal anti-gal-1 antibody (Fig. 1*G*). These data strongly suggest a role for gal-1 in EC biology.

gal-1 Is Required for Coordinated Angiogenesis *in Vivo*. The role of gal-1 in angiogenesis *in vivo* was first studied in the chick chorioallantoic membrane (CAM). Treatment of the CAM with a rabbit polyclonal anti-gal-1 antibody induced a significant inhibition of microvessel density, similar to results published for anginex (4, 5), albeit less pronounced. Interestingly, treatment caused tortuous and irregular growth of the vessels, suggesting a defect in vascular guidance (Fig. 6, which is published as supporting information on the PNAS web site). For further insight in the role of gal-1 during angiogenesis *in vivo*, we used the *Tg(fli1:egfp)^{y1}* zebrafish model. In this model, EC are marked by expression of GFP (17). Recently, three prototype galectins were described in zebrafish (Lgals1-L1, -L2, -L3), of which Lgals1-L2 was found to preferentially bind *N*-acetyllactosamine, similar to human gal-1 (18). Because *Lgals1-L1* is not expressed during embryogenesis (18), we studied only the role of the other two prototype galectins in vascular development. Whole-mount RNA *in situ* hybridization at 48 h postfertilization revealed
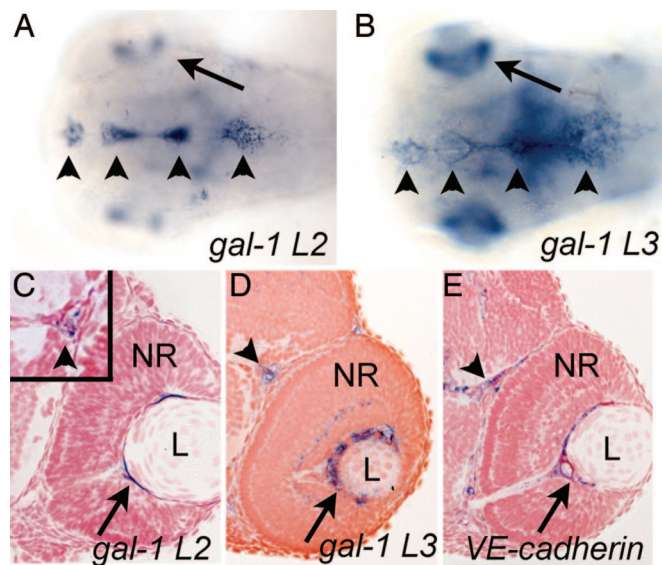
Fig. 2. Expression of zebrafish *Lgals1-L2* and *Lgals1-L3*. Whole-mount *in situ* hybridization on 48-h zebrafish embryos. (*A*) *Lgals1-L2* is strongly expressed in the eyes around the lens (arrow) and in the ventricular zone in the head (arrowheads). (*B*) *Lgals1-L3* expression is less restricted but does overlap with *L2* expression around the lens (arrow) and in the ventricular zone (arrowheads). (*C–E*) Cross-sections at the level of the midbrain of whole-mount *in situ* hybridizations of *Lgals1-L2* (*C*) (*Inset* is photographed from more anterior section), *Lgals1-L3* (*D*), and *VE-cadherin* (*E*). Expression of both *Lgals1-L2* and *L3* is observed in blood vessels in the brain (arrowhead in *C* and *D*) and the retinal vessels (arrow in *C* and *D*) and colocalizes with the expression of EC marker *VE-cadherin*.

specific expression of *Lgals1-L2* in the eyes around the lens and in the ventricular zone in the head (Fig. 2*A*). *Lgals1-L3* expression was broader and largely overlapped with that of *Lgals1-L2* (Fig. 2*B*). Furthermore, cross-sections at the level of the midbrain showed colocalization of both *Lgals1-L2*, and *-L3* and the EC specific marker *VE-cadherin* in the retinal vessels (Fig. 2 *C–E*) and in the blood vessels in the brain (data not shown).

To determine the function of *Lgals1-L2* and *-L3* on vascular development, morpholino-modified antisense oligonucleotides (MOs) were designed to specifically target either the translation

start site (ATG-MO) or the splice donor site (splice-MO). We verified that injection of each splice-MO successfully interfered with the splicing of the respective transcripts (data not shown). Injection of either *Lgals1-L2* or *-L3* ATG-MO induced hemorrhages in the head and in or behind the eyes of the embryos at 2.5 days postfertilization, as detected with a sensitive *o*-dianisidine blood staining. Coinjection of both *Lgals1-L2* and *-L3* MOs resulted in even more severe hemorrhages (Fig. 3 *A–D*). Similar results were observed with the splice-MOs (data not shown). Confocal scanning laser microscopy in the ventricular zone of *Tg(fli1:egfp)^{y1}* zebrafish revealed vascular defects, at the location of the hemorrhages, after coinjection of *Lgals1-L2* and *-L3* ATG-MO. Compared with untreated zebrafish (Fig. 3*F*), abnormal sprouting and misguidance of vessels clearly appeared in the midcerebral area of the *Lgals1-L2* and *-L3* ATG-MO-treated animals (Fig. 3 *E–H*). Vascular network formation of the middle cerebral-, dorsal longitudinal-, mesencephalic-, and anterior cerebral veins was also distorted by both MOs and most severely in the double knockdown (Fig. 3*G*). The same defects were observed upon coinjection of both splice-MOs, indicating specificity of the knockdown defects (Fig. 3*H*), whereas a single injection of each splice-MO revealed weaker defects (data not shown). Similar to those in the ventricular zone, retinal vessels showed abnormal sprouting and growth in the regions where hemorrhages occurred (data not shown). Together with observations from the CAM, results in zebrafish indicate that gal-1 is important *in vivo* for coordinated vessel outgrowth and vascular network formation.

gal-1 Facilitates Tumor Progression Through Angiogenesis. The presented results urged us to study the role of gal-1 by analyzing tumor angiogenesis in gal-1-null mice (19). To compare tumor growth in the presence or absence of gal-1, wild-type (gal-1$^{+/+}$) and null (gal-1$^{-/-}$) mutant 129P3/J mice were s.c.-injected with syngeneic murine F$_9$ teratocarcinoma cells. Three days after injection, a small palpable tumor developed in all mice, suggesting that tumor initiation and initial growth do not depend on gal-1. However, subsequent tumor growth was significantly abrogated in the gal-1$^{-/-}$ mice compared with the wild-type animals. Fifteen days after injection, the tumor volumes in the gal-1$^{-/-}$ mice were ≈4-fold smaller compared with those in the gal-1$^{+/+}$ mice (Fig. 4*A*). As expected, immunohistochemical analysis showed high expression of gal-1 in the EC of tumor vessels in wild-type animals and no expression in null mice (Fig.

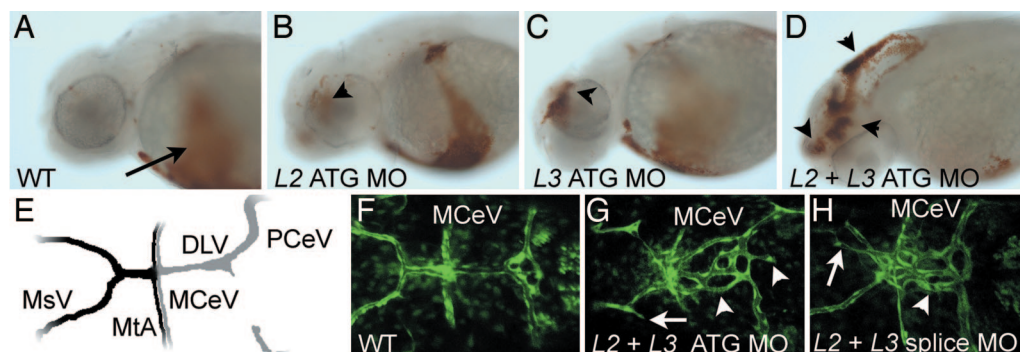**Fig. 3.** Loss of zebrafish gal-1 L2 and L3 results in hemorrhages in the brain and defective vessel formation. (*A–D*) *o*-Dianisidine staining for hemoglobin on 2.5 days postfertilization (dpf) embryos. Wild-type control (*A*) or injected with *Lgals1-L2* AT-MO (*B*), *Lgals1-L3* ATG-MO (*C*), or both *Lgals1-L2* and *-L3* ATG-Mos (*D*). Coinjection of *L2* and *L3* ATG-MO results in severe hemorrhaging in the brain region (arrowheads). Arrow in *A* shows blood accumulating on the yolk and in the heart of a control embryo. (*E*) Schematic drawing of blood vessels in the dorsal brain at 2.5 dpf (modified from ref. 46). (*F–H*) Projection of Z-stacks made by confocal microscopy from *Tg(fli1:egfp)^{y1}* transgenic embryos at the level of the dorsal brain vessels at 2.5 dpf. (*F*) Wild-type control embryo. (*G*) Embryos coinjected with *Lgals1-L2* and *-L3* ATG-MO display aberrant sprouting and misguidance of the middle cerebral vein (MCeV) into the dorsal longitudinal vein (DLV; arrowheads). Defective angiogenic sprouting is also observed in the mesencephalic vein (arrow). (*H*) Coinjection of the *Lgals1-L2* and *-L3* splice-MO shows similar defects in angiogenic sprouting of the brain vessels. DLV, dorsal longitudinal vein; MCeV, middle cerebral vein; MsV mesencephalic vein; MtA, metencephalic artery; and PCeV, posterior cerebral vein.
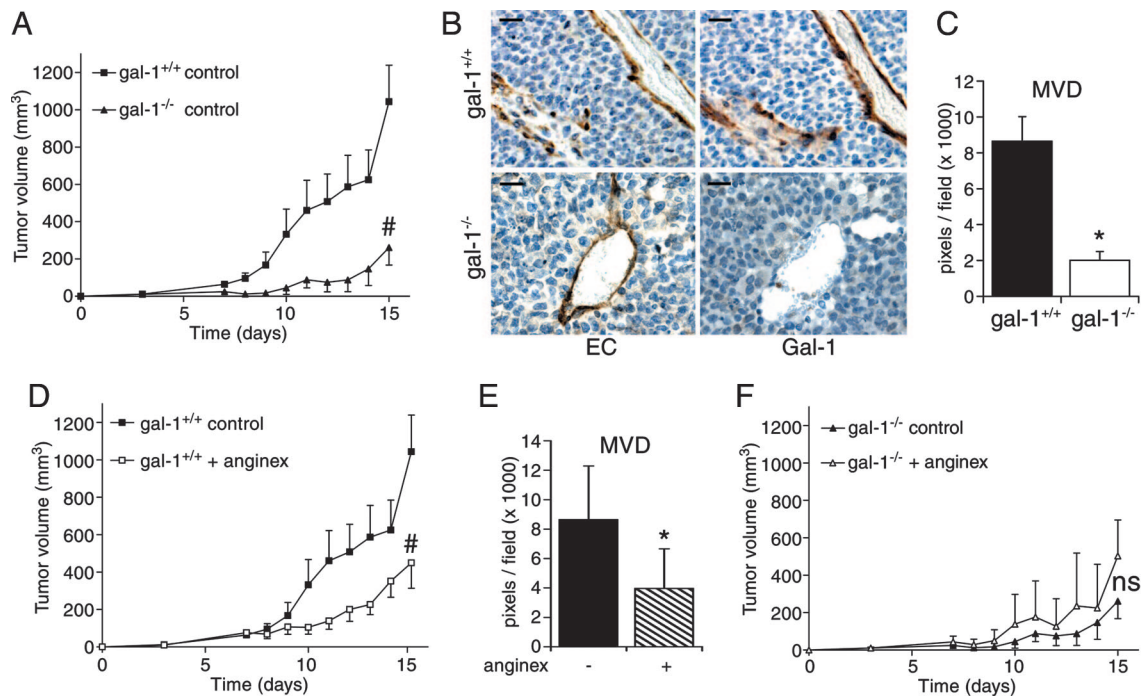
Fig. 4. Hampered tumor growth and lack of responsiveness to anginex in gal-1-deficient mice. (*A*) F_9 teratocarcinoma tumor growth in gal-1$^{+/+}$ (filled squares) and gal-1$^{-/-}$ (filled triangles) mice. #, $P < 0.001$. (*B*) Immunohistochemical evaluation of vasculature and gal-1 expression in tumors from gal-1$^{+/+}$ (*Upper*) and gal-1$^{-/-}$ (*Lower*) mice. (*Left*) Vessel staining with EC marker 9F1 (brown). (*Right*) gal-1 staining (brown) is shown in consecutive sections. (Scale bar, 20 μm.) (*C*) Quantification of microvessel density (MVD) in tumors from gal-1$^{+/+}$ (black bars) and gal-1$^{-/-}$ (white bars) mice. *, $P < 0.001$ vs. wild-type mice. (*D*) F_9 teratocarcinoma tumor growth in gal-1$^{+/+}$ mice during treatment with PBS (filled squares) or anginex (open squares). #, $P < 0.001$ vs. control. (*E*) Quantification of MVD in gal-1$^{+/+}$ mice after treatment with PBS or anginex. *, $P < 0.05$ vs. untreated. (*F*) F_9 teratocarcinoma tumor growth in gal-1$^{-/-}$ during treatment with PBS (filled triangles) or anginex (open triangles). ns, nonsignificant.

4*B*). Quantification of microvessel density revealed a significantly lower amount of blood vessels in null compared with wild-type mice (Fig. 4*C*). In addition, parameters of vessel architecture were decreased (Table 2, which is published as supporting information on the PNAS web site). Because gal-1 has been shown to mediate apoptosis in activated T cells, which could contribute positively to tumor growth (20), we also quantified the amount of peripheral blood leukocytes and the presence of CD45$^+$ and CD8$^+$ cells in the tumors. There was no significant difference in these parameters between gal-1$^{+/+}$ and gal-1$^{-/-}$ animals (Fig. 7, which is published as supporting information on the PNAS web site), which strongly suggests that, in this particular model, impaired tumor progression in gal-1-null mice largely results from decreased angiogenesis.

gal-1 Is a Target Protein for Angiostatic Therapy. Because gal-1 was initially identified as a receptor for the angiostatic peptide anginex, we also analyzed the effect of anginex treatment in wild-type and gal-1-null mice. In wild-type animals, anginex significantly inhibited tumor growth by ≈70% (Fig. 4*D*) and vessel density by ≈55% (Fig. 4*E*), which is comparable with previous observations for anginex in other tumor models (5, 21). In gal-1$^{-/-}$ mice, treatment with anginex had no effect on tumor growth (Fig. 4*F*). In addition, anginex treatment did not significantly affect the number of infiltrating CD45$^+$ or CD8$^+$ cells in the tumors of both the wild-type and null mice (Fig. 8, which is published as supporting information on the PNAS web site). These data demonstrate that gal-1 mediates the angiostatic activity of anginex, and that gal-1 can serve as a target for angiostatic therapy.

Discussion

The current study demonstrates that gal-1 is important in tumor angiogenesis, and that targeting of gal-1 can be an efficient

angiostatic therapeutic strategy. Previous studies have shown that gal-1 is key in two mainstays of cancer. First, gal-1 supports metastasis formation, because it facilitates interactions between tumor cells and EC (22, 23). Second, it protects the tumor against immunity, because it can induce apoptosis in tumor-infiltrating cytotoxic leukocytes (14, 20). This study now reports a critical role in angiogenesis, a third important pillar in tumor growth. Our results reveal a direct role of gal-1 in EC biology. We found a direct involvement of gal-1 in EC proliferation and migration *in vitro* and tumor angiogenesis *in vivo*. Although the angiogenesis-independent onset of F_9 tumor growth was similar in gal-1-null and wild-type mice, the angiogenesis-dependent outgrowth of tumors was severely hampered in the null mice. The low microvessel density in the null mice led us to conclude that the abrogated tumor growth is caused by inefficient angiogenesis. It has been shown that gal-1-null mice have subtle neuronal abnormalities that become apparent upon challenge (24, 25). In line with this, the effect on angiogenesis also becomes apparent by challenging the mice with a growing tumor. This corroborates with our observations in the CAM and the zebrafish, in which acute interference with gal-1 function also results in aberrant angiogenesis. Obviously, the presence of gal-1 is required for a proper response to an acute stress or pressure on EC biology and angiogenesis. It remains to be investigated whether vascular development in the null mice is indeed normal, or whether subtle vascular defects do exist.

We also observed that intervening with gal-1 function results in irregular patterning of the vasculature. The abnormal vessel architecture in the CAM, the zebrafish model, and knockout mice tumors suggests that gal-1 is involved in vascular network formation. Recent studies have shown that the development of both vascular and neuronal networks is regulated by the same receptor/ligand pairs, i.e., Robos/Slits, Ephrins/Eph receptors,

Neuropilins/Semaphorins, and Netrins/Unc5B (26, 27). Interestingly, for gal-1, a role in neuronal pathfinding has already been identified (28). Furthermore, gal-1-null mice show neuronal abnormalities in adulthood (25). Together with the role of gal-1 in angiogenesis described here, these data strongly suggest that gal-1, as well as other members of the galectin family [galectin-3 (29, 30)], is also involved in both neuronal and vascular development.

It has been proposed that galectins can serve as molecular targets for cancer therapy (20, 31–33). Interestingly, we identified gal-1 as a receptor for the angiostatic peptide anginex. Anginex has been shown to inhibit tumor growth by inhibition of tumor angiogenesis (4–6). A previous study reported that transport to the tumor vasculature is facilitated by fibronectin (34). Our results now show that for the angiostatic activity on EC, gal-1 is required. Anginex treatment in gal-1-null mice did not result in further inhibition of the already hampered tumor growth, whereas wild-type mice responded as reported (5, 6). This observation indicates that gal-1 is essential for the activity of anginex, and that gal-1 can indeed serve as a target for angiostatic cancer therapy. We also observed high expression of gal-1 in EC in mouse tumors as well as in human colon and breast carcinomas. There are other reports on the expression of gal-1 in tumor stroma, mainly in studies comparing the expression between normal and cancerous tissues (reviewed in ref. 33). Elevated stromal expression of gal-1 has been reported in several cancers, including cancer of the ovaries (35), breast (36), prostate (37), and colon (38). These results suggest that the increased expression in tumors makes the protein an excellent target for diagnostic or therapeutic purposes.

It is attractive to speculate that, because gal-1 is crucial in several prerequisites for unlimited tumor growth, gal-1-targeting compounds may have multimodal activities. Interfering with gal-1 function could (*i*) prevent metastasis formation through inhibition of gal-1-facilitated tumor cell–EC interactions (22, 23), (*ii*) abrogate tumor escape from immunity through blockade of gal-1-induced apoptosis in activated T lymphocytes (14, 20), and (*iii*) prevent the execution of tumor angiogenesis (this work). This multifunctionality makes gal-1 an excellent target for cancer therapy.

Materials and Methods

Cell Cultures. HUVEC and the human microvascular EC line HMEC were cultured as described (5). F$_9$ teratocarcinoma cells (kind gift from H. Weich, German Research Center for Biotechnology, Braunschweig, Germany) were cultured in RPMI medium 1640 supplemented with 10% FBS/1% glutamin/50 units/ml penicillin/50 ng/ml streptomycin.

Mouse Tumor Model. A total of 14 adult 129P3/J gal-1$^{-/-}$ mutant mice (19) and 17 matched 129P3/J gal-1$^{+/+}$ (wild-type) mice were used in this study. On day 1, animals were injected s.c. with 3×10^6 syngeneic F$_9$ teratocarcinoma cells. On day 7, anginex treatment (10 mg/kg per day) was started in seven wild-type and nine mutant mice by daily i.p. injections. Tumor volume and mouse weight were measured daily throughout the experiment. Animals were given water and standard chow ad libitum, and they were kept on a 12-h light/dark cycle. All experiments were approved by the local ethical review committee.

Knockdown of gal-1 Expression *in Vitro*. Knockdown of gal-1 expression *in vitro* was obtained by using a gal-1-specific antisense ODN (hgal1 ODN: GTCACCGTCAGCTGCCATGT). As control, a random nonspecific antisense ODN (control ODN: TCCCTAGTGACTCTTCCC) was used. ODNs were renewed every other day.

FACS Analysis. FACS analysis of gal-1 protein expression was performed on ethanol-fixed HUVEC. Cells were washed in 0.1% BSA/0.01% sodium azide/PBS, incubated on ice with polyclonal rabbit anti-galectin antibody (39), and washed with PBS. Next, the cells were incubated with FITC-labeled polyclonal goat anti-rabbit Ig antibody (Dako, Carpenteria, CA) and washed with PBS. Five thousand events were acquired for each sample on a FACSCalibur flow cytometer (Beckton Dickinson, Franklin Lakes, NJ). All experiments were performed in triplicate.

Migration, Proliferation, and CAM Assays. Migration, proliferation, and CAM assays were performed as described (16). Within each proliferation experiment, treatments were done in triplicate, and all proliferation and migration experiments were performed at least three times. For the CAM, two independent experiments were performed (overall $n = 13$ per treatment group).

Real-Time PCR. Total RNA isolation, subsequent cDNA synthesis, and real-time PCR were performed as described (40) with primers targeted against human gal-1 (forward: TGCAACAG-CAAGGACGGC; reverse: CACCTCTGCAACACTTCCA). Primers were purchased from Eurogentec (San Diego, CA), and experiments were performed in triplicate.

Immunohistochemistry. Immunohistochemical staining of anginex uptake was performed on HUVEC cytospins. Cells were acetone-fixed and air-dried. After incubation in 1% paraformaldehyde, cells were incubated in FCS, after which mouse 2D10 monoclonal antianginex antibody (5) was applied in 0.05% Triton X-100/PBS. After incubation with Texas red-labeled goat–anti-mouse Ig antibody, cells were washed with PBS and mounted in Immumount (Shandon, San Jose, CA) supplemented with 1 µg/ml DAPI (Molecular Probes, Eugene, OR). In the negative control, incubation with the first antibody was omitted.

Double staining for Ki67 and CD31/34 on paraffin-embedded tissue sections was performed as described (41). Tissues from normal colon, colon carcinoma, and Ewing sarcoma were obtained from the stocks of the Department of Pathology, University Hospital Maastricht. For gal-1 staining, paraffin-embedded tissue sections were dewaxed, and endogenous peroxidase activity was blocked with 0.3% H$_2$O$_2$ in methanol. Next, the slides were microwave pretreated in citric acid. After blocking with 1% BSA/PBS, primary antibody was applied in 0.5% BSA/PBS. Next, biotin-labeled secondary antibody was applied, and staining was performed with the StreptABComplex/HRP kit (Dako) according to the supplier's protocol. The tissue sections were counterstained with haematoxylin (Merck, Whitehouse Station, NJ), dehydrated, and mounted in Entellan (Merck). The same protocol was used for EC staining with the EC-specific antibody 9F1 (42). Staining for CD45+ and CD8+ cells was performed on frozen tissue sections fixed in acetone and air-dried. Endogenous peroxidase activity was blocked with 0.3% hydrogen peroxidase/PBS, and aspecific binding was blocked with 20% FCS/0.1% Tween20/PBS. Next, the primary antibody (MP33 rat anti-mouse CD45 or 53.6.27 rat anti-mouse CD8) was applied, followed by incubation with biotin-labeled secondary antibody. Staining was visualized by using the Vectastain ABC kit (Vector Laboratories, Burlingame, CA), and subsequently sections were counterstained with haematoxylin, dehydrated, and mounted with Entellan. Within each section, the number of positive cells was scored at four different locations in a blinded fashion by two different observers. Fluorescent staining of CD31 in murine tumors and subsequent scoring of vessel characteristics were performed as described (6).

Zebrafish Experiments. For *in vivo* experiments, the previously described *Tg(fli1:egfp)^{y1}* zebrafish was used (17). Knockdown of

Lgals1-L2 and *-L3* expression was achieved by injection of specific MOs (Gene Tools, Philomath, OR) into one-cell stage embryos (43). The following MOs were used: *Lgals1-L2* ATG-MO, 5′-GTATAAGCACACCGGCCATTTTGAC-3′; *Lgals1-L3* ATG-MO, 5′-AAGATCCCAGGCTAAGGACGTCATT-3′; *Lgals1-L2* splice-MO, 5′-TTGTAATATACTCACGGCCATTTTG-3′; *Lgals1-L3* splice-MO, 5′-ATGTCTGTACTCACGCATCA-CAGCC-3′. Before 24 h postfertilization, 1-phenyl-2-thiourea (0.002%) was added to prevent pigment development. For imaging, dechorionated embryos were anesthetized with 0.003% tricaine methanesulfonate and mounted in 2% low melting agarose. Confocal scanning microscopy was performed by using a Leica (Deerfield, IL) TCS NT.

For whole-mount blood staining, dechorionated and 1-phenyl-2-thiourea-treated embryos were incubated in 40% EtOH/0.01 M NaAc, pH5.2/2.0% H_2O_2, in the presence of 0.8 mg/ml *o*-dianisidine. After rehydration in a graded series of EtOH/PBST, the embryos were stored in 50% glycerol at 4°C.

Whole-mount *in situ* hybridization on zebrafish embryos was carried out as described (44). For *VE-cadherin* riboprobe synthesis, we used the previously published plasmid (45). For *Lgals1-L2* antisense-probe synthesis, RZPD clone IMAGp998D0710947Q3 (in pSPORT1) was linearized with BamHI and transcribed with T7 RNA polymerase. Zebrafish *Lgals1-L3* was cloned from RZPD clone IMAGp998J1712051Q3 into pBluescript KS, giving rise to *lgal1-L3*/pBs. For *lgal1-L3* antisense-probe synthesis, plasmid *lgal1-L3*/pBs was linearized with *Acc*65I and transcribed with T7 RNA polymerase. For sectioning, the embryos were embedded in Technovit 8100 (Heraeus Kulzer, Wehrheim, Germany). Seven-micrometer-thick sections were cut and counterstained with neutral red dye.

Statistics. All data are shown as mean with standard error, except where indicated. Data from *in vitro* proliferation, real-time PCR, CAM assay, FACS analysis, and CD45/CD8 scores were analyzed by using the Mann–Whitney U test. Tumor growth curves and migration assay data were analyzed by using two-way ANOVA. Student's t test was used to analyze the vascular parameters. All values are two-sided, and P values <0.05 were considered statistically significant. Two-way ANOVA was performed in GraphPad Prism 3.0 (GraphPad, San Diego, CA). All other statistical computations were performed in SPSS 10.0.5. (SPSS, Chicago, IL).

1. Folkman J (1972) *Ann Surg* 175:409–416.
2. Griffioen AW, Molema G (2000) *Pharmacol Rev* 52:237–268.
3. van Beijnum JR, Griffioen AW (2005) *Biochim Biophys Acta* 1755:121–134.
4. Griffioen AW, van der Schaft DW, Barendsz-Janson AF, Cox A, Struijker Boudier HA, Hillen HF, Mayo KH (2001) *Biochem J* 354:233–242.
5. van der Schaft DW, Dings RP, de Lussanet QG, van Eijk LI, Nap AW, Beets-Tan RG, Bouma-Ter Steege JC, Wagstaff J, Mayo KH, Griffioen AW (2002) *FASEB J* 16:1991–1993.
6. Dings RP, van der Schaft DW, Hargittai B, Haseman J, Griffioen AW, Mayo KH (2003) *Cancer Lett* 194:55–66.
7. Drickamer K (1988) *J Biol Chem* 263:9557–9560.
8. Hirabayashi J, Kasai K (1993) *Glycobiology* 3:297–304.
9. Barondes SH, Castronovo V, Cooper DN, Cummings RD, Drickamer K, Feizi T, Gitt MA, Hirabayashi J, Hughes C, Kasai K, *et al.* (1994) *Cell* 76:597–598.
10. Cooper DN (2002) *Biochim Biophys Acta* 1572:209–231.
11. Houzelstein D, Goncalves IR, Fadden AJ, Sidhu SS, Cooper DN, Drickamer K, Leffler H, Poirier F (2004) *Mol Biol Evol* 21:1177–1187.
12. Hughes RC (2001) *Biochimie* 83:667–676.
13. Scott K, Weinberg C (2004) *Glycoconj J* 19:467–477.
14. Perillo NL, Pace KE, Seilhamer JJ, Baum LG (1995) *Nature* 378:736–739.
15. Park JW, Voss PG, Grabski S, Wang JL, Patterson RJ (2001) *Nucleic Acids Res* 29:3595–3602.
16. Brandwijk RJ, Nesmelova I, Dings RP, Mayo KH, Thijssen VL, Griffioen AW (2005) *Biochem Biophys Res Commun* 333:1261–1268.
17. Lawson ND, Weinstein BM (2002) *Dev Biol* 248:307–318.
18. Ahmed H, Du SJ, O'Leary N, Vasta GR (2004) *Glycobiology* 14:219–232.
19. Poirier F, Robertson EJ (1993) *Development (Cambridge, UK)* 119:1229–1236.
20. Rubinstein N, Alvarez M, Zwirner NW, Toscano MA, Ilarregui JM, Bravo A, Mordoh J, Fainboim L, Podhajcer OL, Rabinovich GA (2004) *Cancer Cell* 5:241–251.
21. Dings RP, Yokoyama Y, Ramakrishnan S, Griffioen AW, Mayo KH (2003) *Cancer Res* 63:382–385.
22. Lotan R, Belloni PN, Tressler RJ, Lotan D, Xu XC, Nicolson GL (1994) *Glycoconj J* 11:462–468.
23. Clausse N, van den Brule F, Waltregny D, Garnier F, Castronovo V (1999) *Angiogenesis* 3:317–325.
24. McGraw J, McPhail LT, Oschipok LW, Horie H, Poirier F, Steeves JD, Ramer MS, Tetzlaff W (2004) *Eur J Neurosci* 20:2872–2880.
25. McGraw J, Gaudet AD, Oschipok LW, Steeves JD, Poirier F, Tetzlaff W, Ramer MS (2005) *Pain* 114:7–18.
26. Klagsbrun M, Eichmann A (2005) *Cytokine Growth Factor Rev* 16:535–548.
27. Weinstein BM (2005) *Cell* 120:299–302.
28. Puche AC, Poirier F, Hair M, Bartlett PF, Key B (1996) *Dev Biol* 179:274–287.
29. Nangia-Makker P, Honjo Y, Sarvis R, Akahani S, Hogan V, Pienta KJ, Raz A (2000) *Am J Pathol* 156:899–909.
30. Kuklinski S, Vladimirova V, Waha A, Kamata H, Pesheva P, Probstmeier R (2003) *J Neurochem* 87:1112–1124.
31. Zou J, Glinsky VV, Landon LA, Matthews L, Deutscher SL (2005) *Carcinogenesis* 26:309–318.
32. Liu FT, Rabinovich GA (2005) *Nat Rev Cancer* 5:29–41.
33. van den Brule F, Califice S, Castronovo V (2004) *Glycoconj J* 19:537–542.
34. Akerman ME, Pilch J, Peters D, Ruoslahti E (2005) *Proc Natl Acad Sci USA* 102:2040–2045.
35. Allen HJ, Sucato D, Woynarowska B, Gottstine S, Sharma A, Bernacki RJ (1990) *J Cell Biochem* 43:43–57.
36. Gabius HJ, Brehler R, Schauer A, Cramer F (1986) *Virchows Arch B Cell Pathol Incl Mol Pathol* 52:107–115.
37. van den Brule FA, Waltregny D, Castronovo V (2001) *J Pathol* 193:80–87.
38. Lotan R, Matsushita Y, Ohannesian D, Carralero D, Ota DM, Cleary KR, Nicolson GL, Irimura T (1991) *Carbohydr Res* 213:47–57.
39. Pace KE, Hahn HP, Baum LG (2003) *Methods Enzymol* 363:499–518.
40. Thijssen VL, Brandwijk RJ, Dings RP, Griffioen AW (2004) *Exp Cell Res* 299:286–293.
41. de Lussanet QG, Backes WH, Griffioen AW, Padhani AR, Baeten CI, van Baardwijk A, Lambin P, Beets GL, van Engelshoven JM, Beets-Tan RG (2005) *Int J Radiat Oncol Biol Phys* 63:1309–1315.
42. Harder R, Uhlig H, Kashan A, Schutt B, Duijvestijn A, Butcher EC, Thiele HG, Hamann A (1991) *Exp Cell Res* 197:259–267.
43. Nasevicius A, Larson J, Ekker SC (2000) *Yeast* 17:294–301.
44. Hammerschmidt M, Pelegri F, Mullins MC, Kane DA, Brand M, van Eeden FJ, Furutani-Seiki M, Granato M, Haffter P, Heisenberg CP, *et al.* (1996) *Development (Cambridge, UK)* 123:143–151.
45. Larson JD, Wadman SA, Chen E, Kerley L, Clark KJ, Eide M, Lippert S, Nasevicius A, Ekker SC, Hackett PB, Essner JJ (2004) *Dev Dyn* 231:204–213.
46. Isogai S, Horiguchi M, Weinstein BM (2001) *Dev Biol* 230:278–301.